Process Safety and Environmental Protection 190 (2024) 198–210

Contents lists available at ScienceDirect

Process Safety and Environmental Protection

journal homepage: www.journals.elsevier.com/process-safety-and-environmental-protection

Water transport and corrosion under insulation: Experimental investigations of drying in mineral wool

Hristina Dragovic [a], Daniela S. Damaceno [b], Ole H.H. Meyer [b], Åsmund Ervik [b,*]

[a] Norwegian University of Science and Technology, Trondheim 7034, Norway
[b] SINTEF Energy Research, Trondheim 7034, Norway

ARTICLE INFO

Keywords:
Corrosion under insulation
CUI
Humidity transport
Mineral wool
Vertical hot pipe
Time of wetness

ABSTRACT

Corrosion under insulation (CUI) is a major risk factor for the material integrity of insulated equipment that is encountered i.a. in the chemical process industries. Undetected CUI has been the root cause for major accidents, including loss-of-site, loss-of-life, prolonged plant shutdown, and environmental pollution. Reducing CUI risk via labour-intensive inspection routines is associated with billions of dollars of annual maintenance costs worldwide. CUI is caused by water bypassing a weather shield, migrating through the insulation and contacting the equipment surface. The resulting corrosion rates are very high and the process is hidden from view. Surprisingly, the fundamental mechanisms that drive water migration through insulation have been largely unexplored. In this work we present novel experimental investigations of the evaporation and drying dynamics for a heated vertical pipe with preformed mineral wool insulation and metal cladding. Relative humidity and temperature sensors provide measurements of how the water evaporates and travels through the system during controlled water ingress experiments. The experimental data shows that the drying time of the insulation material is proportional to the amount of water added. We find that the drying process proceeds in two stages, where the length of the first drying regime is directly related to the diffusion-limited evaporation from the bulk liquid water, while the second drying time is influenced also by other factors such as the adsorption and desorption of water on the insulation material fibres. The findings have implications for how time of wetness, used in CUI risk-based inspection methods, can be obtained from humidity sensor data. The new insights into water transport in insulation enables a paradigm shift towards predictive CUI maintenance using humidity spot sensors.

1. Introduction

Corrosion under insulation (CUI) refers to external, often localized, corrosion on the metal surface of insulated process equipment as a result of water ingress in the insulation (de Landtsheer, 2020). In many industries, equipment is insulated to stabilize process temperature, for fire protection or noise reduction. A commonly used insulation system is comprised of an open fibrous material such as hydrophobic mineral wool, that is covered by a metal or plastic cladding to protect from water ingress. However, the cladding is in practice never perfect, allowing water to enter through imperfections or damages in the cladding. Often, the ingressed water may be retained in the insulation material. In this work we specifically study insulated pipes, and for convenience will use the terms “pipe” or “piping”, but the findings and discussions herein will in general apply to other types of insulated equipment such as vessels, valves, tanks etc.

If allowed to progress, CUI leads to integrity issues with major accident potential if the corrosion causes material degradation of equipment that contains flammable or explosive fluids (Anderson, 2010; De Vogelaere, 2009; Langøy et al., 2017). A further aggravating factor is that the insulation can retain the flammable fluid and cause a *lagging fire* (Fu et al., 2021; Brindley et al., 1999). As an example of the consequences of CUI, an explosion and fire that occurred in a refinery caused millions of pounds worth of damage to the facility, where CUI had caused failure in a carbon steel line containing hydrocarbons (Geary, 2013). Another instance of CUI caused a leak in a hydrocarbon transfer line in a refinery close to the Loire river, and resulted in an oil spill of 180 tonnes that contaminated 90 kilometres of coast line and cost 50 million Euros to clean up, cf. ARIA database incident no. 34351. Several engineering failure analyses related to CUI have been published in the open literature, e.g Roffey and Davies (2014)); Kumar et al. (2008)). These failures have significant impact on unplanned maintenance and

* Corresponding author.
E-mail address: asmund.ervik@sintef.no (Å. Ervik).

https://doi.org/10.1016/j.psep.2024.08.016
Received 4 February 2024; Received in revised form 4 July 2024; Accepted 2 August 2024
Available online 5 August 2024

plant downtime, resulting in large costs for facility reparation, and in the worst case injuries and loss of human life (de Landtsheer, 2020).

CUI is known to be a particularly challenging form of corrosion for many reasons. An important factor is that the insulation can hold water and keep the pipe surface exposed to corrosive conditions for extended times, as supported by analysis of corrosion products (Ramirez-Ledesma and Juarez-Islas, 2022). The presence of the insulation material and cladding prohibits direct observation of the pipe surface where corrosion occurs, making it difficult to identify and manage corrosion under insulation. It is possible for CUI to continue undetected (Pojtanabuntoeng et al., 2015) for years or even decades before failure eventually occurs. The current best practice for CUI inspection is full *delagging* (meaning removal) of the cladding and insulation system, and subsequent close visual inspection of the pipe surface (de Landtsheer, 2020). Case history analyses indicate that loss of containment occurs frequently on piping, with CUI thought to be an underlying mechanism (Clay et al., 2020).

Despite the high importance of preventing CUI, there have been limited investigations of how water propagates inside typical insulation systems, and especially, regarding how the water evaporates and leaves the insulation system via convection and diffusion. In the present work we have performed experimental investigations of water evaporation and insulation drying dynamics for a vertical pipe insulated with hydrophobic mineral wool, held in place by a metallic cladding that has a circumferential opening to the ambient air.

In this system, controlled amounts of water are added to a reservoir which is in contact with the pipe wall kept at 70˚C. The relative humidity and temperature of the gas residing within the insulation material is measured by 24 sensors at three different radial positions and 8 different vertical positions. We observe the insulation drying dynamics following addition of liquid water in different quantities, analyse the observations, and compare with a simple one-dimensional model based on diffusion in the vertical direction. A schematic illustrating the experimental setup is given in Fig. 1.

This paper is arranged as follows: In Section 2, we give a brief review of the current understanding of CUI; in Section 3 we review the thermodynamics and transport phenomena of the water-air-insulation system, in Section 4 we describe the setup and methods, in Section 5 we present the results, in Section 6 we discuss the results obtained and in Section 7 we provide concluding remarks.

2. Current understanding of CUI

CUI is a serious problem which affects all types of chemical processing plants, refineries, oil and gas platforms. The issue affects both carbon steel and stainless steel piping, where the latter is prone to chloride-induced stress corrosion cracking. The necessary inspection and maintenance for prevention of CUI related damage constitutes a significant amount of the maintenance budget, and 80 % of CUI events are found on pipes (Fitzgerald et al., 2003). Based on CUI inspection case histories and industry experience, the majority of damage occurs in the *process temperature* range between − 4˚C and 175˚C (de Landtsheer, 2020). It is important to note here that inspection reports frequently cite the nominal, or design-, process temperature, while the actual temperature of the fluid inside the equipment is not known and could be lower. Furthermore, if the equipment is made of low heat capacity material and is subject to low (internal) flow rates, the exterior wall temperature could be significantly below the nominal/design process temperature. This can indicate why CUI may also be encountered when the reported process temperature is above the boiling point of water.

Another challenging aspect of CUI is the, to the best of our knowledge, limited number of research studies on the fundamental aspects of CUI. Most studies do not emphasize the importance of the transport mechanisms of water in insulation materials. Presently, it is not possible to predict reliably where CUI may occur.

Inside the insulation system, at least the following transport mechanisms for water are possible and graphically summarized in Fig. 2: a) liquid water in the insulation or at the inside of the cladding can flow downwards in the system, b) water vapour can move by diffusion down concentration gradients, c) liquid water can propagate through the insulation material by capillary action, d) water can propagate through thin films adsorbed onto the insulation material fibres, e) water vapour can condense into liquid as a result of diffusive transport towards the cold cladding, f) evaporation of liquid into water vapour after liquid has been transported towards the hotter surface. Specifically, in the case of insulated high-temperature pipe systems, a conventional view is that water can propagate in a liquid state to the hot metal (pipe-) surface, evaporate, propagate towards the colder cladding, and condense there. Persisting in a cyclic behaviour, this can lead to accelerated corrosion (de Landtsheer, 2020). At present, the relative importance of the mechanisms a)-f) is not clear.

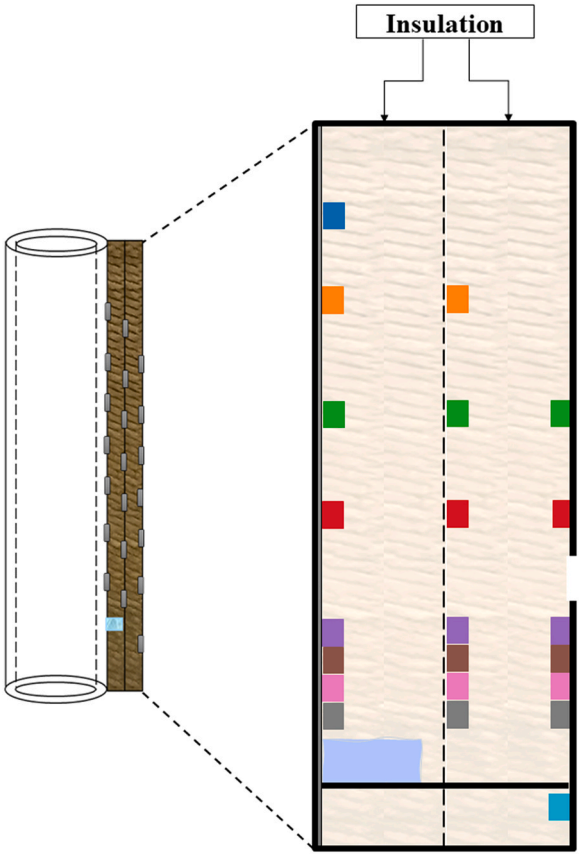

Fig. 1. Illustration of the experimental setup for measuring the evaporation and drying dynamics following water ingress under mineral wool insulation on a vertical pipe. The differently coloured squares indicate the positions of the sensors that measure relative humidity and temperature within the instrumented cross-section.

In this work we study directly the mechanisms b), e) and f). In our experimental setup, liquid water is added directly to a reservoir at the hot surface, such that mechanisms a) and c) are eliminated. Mechanism d) can occur in our system, and is thought to be of relatively minor importance, but can not be measured directly to distinguish it from mechanism b).

In addition to a limited knowledge of the relative importance of water transport mechanisms, there is also uncertainty about whether liquid water presence at the pipe surface is necessary for corrosion (or coating degradation) to occur, or if the presence of high-humidity air in the insulation close to the pipe is sufficient to cause adsorption of water films and corrosion damage. For comparison, in atmospheric corrosion it has been observed that “corrosive wetness” (i.e. establishment of

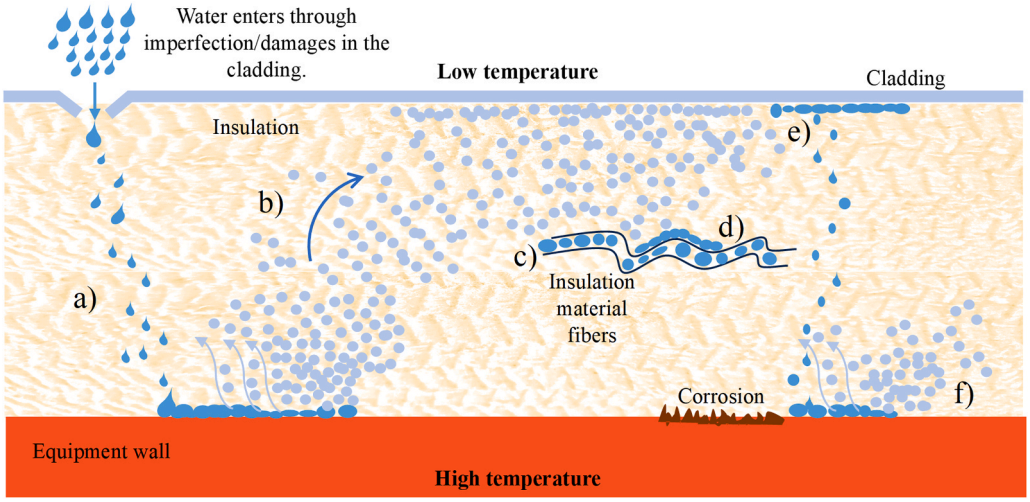

Fig. 2. Illustration of the possible transport mechanisms of water inside the insulation material: a) liquid flowing due to gravity, b) diffusion of water vapour, c) liquid flowing due to capillary action, d) adsorption of water onto fibres, e) condensation of water vapour, f) evaporation of liquid water.

corrosion conditions) can correspond to exposure to an atmosphere with relative humidity as low as 40 % in particular conditions (Mansfeld, 1979). The typical definition in atmospheric corrosion is to take the *time of wetness* as the duration of time the equipment surface is exposed to relative humidity above 80 % at a temperature above 0°C (Roberge, 2008). In addition to the time of wetness, it has been reported that cyclic operating conditions, i.e. repeated drying and wetting of the metal surface, can enhance corrosion, as the corrosion rate is highest just before the surface dries out (Yadav et al., 2004). As far as we are aware, no systematic study on how humidity affects corrosion rates for metal surfaces covered by insulation exists. Presently, it is not clear how observations of atmospheric corrosion can be applied to CUI conditions. The term *time of wetness* is currently used for CUI without any precise definition.

Some previous authors have conducted experimental tests of corrosion rates for CUI. Caines et al. (2015) performed experiments to develop correlations to predict the CUI rate under natural environmental conditions for offshore applications, using an accelerated CUI test in the laboratory (G189, 2007), combined with field testing. Caines et al. (2013); Hillier et al. (2021) focused on the investigation of pitting corrosion behaviour, perhaps the most common type of localized corrosion under insulation in marine environments. Is is found that general corrosion model predictions are not applicable to insulated equipment due to the significant differences in the corrosion mechanism caused by the insulation material (Caines et al., 2017). A clear finding from laboratory studies is that the insulation presence increases the corrosion rate under the insulation compared to non-insulated systems due e.g. to the insulation keeping the moisture longer at the metal surface. In these laboratory studies, large amounts of liquid water were used to thoroughly soak the insulation. It remains an open question how the corrosion rates develop as the water content in insulation decreases, especially in the presence of a strong thermal gradient.

One of the most effective measures for preventing corrosion of the equipment is to use a protective coating material (de Landtsheer, 2020). Selection of coating materials is done according to the equipment material, operating temperature cycles etc. The resistance of a given coating to different salt solutions as well as salt sprays is typically used to assess coating performance. For a review of the different types of coatings, see e.g. the articles by (Miyashita, 2017; Miyashita et al., 2016; Kane et al., 2008). What is important to note is that all coating systems will eventually degrade when immersed in water, and that current risk-based inspection methods have to assume that the coating will be permanently immersed in water. This means that knowledge of whether the equipment surface is wet or dry can drastically improve the accuracy of predicting the remaining lifetime of the coating. Different technical solution have also been investigated to protect the equipment surface from water and reduce the drying time of the insulation material once it becomes wet. Contact-free systems are designed with an air gap preventing direct contact of the wet insulation material and metal (Rana et al., 2021; Haraldsen, 2010) and have been applied with success in recent years. Similarly, solutions exist where the air gap is designed between the insulation material and the cladding, where the goal is to prevent the outside of the insulation material to be exposed to liquid that is condensing during periods with low ambient temperatures. These solutions are typically used together with drain holes in the cladding to allow liquid to flow out and to reduce the insulation dry-out time by allowing the diffusion of water vapour entrapped inside the insulation material. For instance, in the NORSOK Standard M004 “Piping and Equipment insulation” it is recommended to deploy drainage holes with a minimum diameter of 16 mm located at the 6 o’clock position on horizontal pipe runs with a spacing of maximum 2 m.

The influence of drain holes in the cladding on the drying of the insulation material was investigated by Pojtanabuntoeng et al. (2015)), but is a topic that needs further exploration. It is clear that larger drain holes increase the exchange of humid air with the ambient. However, larger openings also increase the possibility for water ingress, such that a balance of these factors must be considered. In the present work the opening in the cladding has a fixed area. Further research is needed on the impact of varying the sizes of drain holes.

The difficulties in predicting CUI are the main motivation for the development of risk-based inspection strategies. These are dependent on estimates for the corrosion rate. In the idealized case of dry insulation, the risk of CUI is set to be negligible (de Landtsheer, 2020). In practice, this is never the case for outdoor equipment, and inspection of the pipe surface is necessary for CUI risk classification. Sophisticated non-destructive inspection (NDI) methods to assess the corrosion rate or wetness state under the insulation exist, (Cao et al., 2022): ultrasonic inspection (Zhu et al., 1998), pulsed eddy current (Sophian et al., 2017; Cheng, 2012; Brett and Raad, 1996; Angani et al., 2010), neutron backscatter (Hart, 2014), microwaves (Jones et al., 2012; Simonetti et al., 2015), and sniffing dogs trained on the scent of corrosion (Schoon et al., 2014). NDI is generally a complex inspection operation, and particularly challenging for complex geometries or at elevated locations. NDI techniques provide information on a single point in time to give a snapshot of the equipment integrity, and cannot anticipate corrosion that will happen in the future, and therefore cannot be used to predict CUI before it occurs (Fransen et al., 2018).

As the presence of water in the insulation is generally believed to be

the main prerequisite for CUI, a different approach is to implement a monitoring solution that detects water in the insulation. In particular, the concept of measuring the water content in the air inside the insulation by relative humidity spot sensors has been proposed (Fransen et al., 2018). Further knowledge about the fundamentals of water vapour transport in porous insulation materials is needed to enable the application of a spot sensor humidity detection system.

Understanding of humidity migration in insulation materials is mainly derived from energy gains and losses calculations in building physics (Tariku et al., 2010a). In building physics, however, one commonly assumes that the temperature has no influence on humidity transport. In building physics applications, temperature differences (and gradients) across the insulation layer are generally significantly lower than compared to typical CUI conditions. Philip and Vries (1957)) investigated the influence of temperature gradients on humidity transport in porous materials by modelling of diffusion. The occurrence of mould formation in building structures (in the vicinity of localized humidity concentration peaks and due to inappropriate insulation ventilation for material drying-out), can be compared with a corrosion process that is developing under humid insulation. Numerical models for humidity transfer in porous building materials have been developed and applied by Hagentoft et al. (2004)); Belleudy et al. (2016)); Shrestha et al. (2021)); Tariku et al. (2010b)) to identify humidity profiles in building materials. Liquid water transport mechanisms in porous building materials can be described using water sorptivity measurements through free water intake experiments (Vejmelková et al., 2009; Hall, 1977, 1989; Ioannou et al., 2008; Yang et al., 2006; Hall and Tse, 1986; Roels et al., 2004). Water ingress into hydrophilic insulation material, such as older types of mineral wool, increases the insulation material thermal conductivity, causing reduction in insulation performance. Then, undesired variations in the optimized process temperature can occur (Hoffman, 2019; Jerman and Černý, 2012; Jiričková and Černý, 2006). Effects of convection inside insulation is mostly related to highly permeable materials (Dyrbøl et al., 2002).

In this work, we seek to improve understanding of the relation between insulation material drying time and the amount of added water to the system by means of experiments, simple theoretical modelling of diffusion processes, and identification of other transport mechanisms that affect the system dry-out time. The findings from this contribution support the development of sensor based humidity monitoring technologies, enabling predictive CUI maintenance.

3. Theory

3.1. Thermodynamics of humid air

For the temperatures and pressures that are relevant in CUI applications, humid air can be considered as an ideal gas mixture of dry air and water vapour, such that Dalton's law of partial pressures is applicable. The vapour pressure of water is then given by the ideal gas law,

$$Mp_v = \rho_v RT, \tag{1}$$

where M is the molar mass of water vapour, p_v is the vapour pressure, ρ_v is the density of water vapour, R is the universal gas constant, and T is the temperature. The total pressure p is given by the sum of the vapour pressure and the partial pressure of dry air, p_d,

$$p = p_d + p_v. \tag{2}$$

The specific humidity, Y_w, is defined as the mass of water vapour m_{H_2O} per unit mass of humid air m (or mass fraction of water vapour in the gas mixture):

$$Y_w = \frac{m_{H_2O}}{m} = \frac{m_{H_2O}/V}{m/V} = \frac{\rho_v}{\rho}, \tag{3}$$

where V is a control volume enclosing humid air with density ρ and mass m. Specific humidity is equal to the ratio of the partial density of water vapour ρ_v to the total density of humid air ρ. Moreover, the specific humidity is related to absolute humidity through the water vapour density ρ_v. The absolute humidity AH is defined by the mass of water vapour m_{H_2O} per humid air volume V, and is related to the specific humidity,

$$AH = \frac{m_{H_2O}}{V} = \rho_v = Y_w \rho. \tag{4}$$

The saturation vapour pressure $p_{sat}(T)$ is defined as the vapour pressure at the gas-liquid interface in a state of equilibrium; here at the (flat) surface of a pool of liquid water. The dependence of saturation vapour pressure on temperature can be described by the Clausius-Clapeyron equation (Petty, 2008). A particular solution of the Clausius Clapeyron equation is the Magnus equation (Buck, 1981), which relates saturation vapour pressure to temperature for humid air:

$$p_{sat}(T) = 6.112 \exp\left(\frac{17.62T}{243.12 + T}\right), \tag{5}$$

where T is the temperature in ˚C, and the empirical parameters in the equation are valid for water vapour. The saturation vapour pressure is a monotonically increasing function of temperature.

The relative humidity RH is then given by the actual vapour pressure p_v expressed as a fraction of the saturation vapour pressure $p_{sat}(T)$:

$$RH = \frac{p_v}{p_{sat}(T)}. \tag{6}$$

Applying the ideal gas law to partial water vapour pressure p_v, the absolute humidity (Eq. (4)) can also be related to the vapour pressure. The absolute humidity at which the gas is saturated AH_{sat} can be determined using the ideal gas law and the saturated vapour pressure in Eq. (5):

$$AH_{sat} = \frac{Mp_{sat}}{RT}. \tag{7}$$

Hence, the relative humidity can be understood as the ratio of absolute humidity to the absolute humidity at which the gas is saturated,

$$RH = \frac{AH}{AH_{sat}}. \tag{8}$$

The specific humidity Y_w can then be calculated from the temperature and relative humidity measurements according to

$$Y_w = RH \frac{Mp_{sat}(T)}{\rho(RH, T)RT} \tag{9}$$

where the ideal gas law can be used to calculate $\rho(RH, T)$.

3.2. Adsorption and absorption of gases on solids

Adsorption is a spontaneous process that decreases the surface energy of solids in contact with gases by having gas molecules stick to the solid surface. For mono-layer adsorption the phenomena are well represented by the Langmuir adsorption isotherm (Kontogeorgis and Kiil, 2016), while for multi-layer adsorption more advanced models such as the BET equation can be employed. The adsorbed phase for humid air will predominantly consist of water molecules. In addition to adsorption at the solid surface, absorption further into the bulk of the solid can occur.

Mineral wool is a material that has a high permeability, high porosity and low water adsorption compared to more commonly studied materials such as wood or concrete. For instance Jerman and Černý (2012), (Jiričková and Černý, 2006) performed measurements of adsorption isotherms for mineral wool. The amount of water adsorption in mineral wool is low compared to e.g. wood, where even dry wood can contain more than 10 % water by volume. Even so, the amount of adsorbed

water in the insulation can be significantly larger than the amount of water in the humid air inside the insulation, such that the adsorbed water films can provide a significant reservoir for water during wetting and drying phenomena.

Absorption of water is the working principle of typical inexpensive commercially available humidity sensors. These work based on the plate capacitor principle with a thin polymer layer that absorbs water molecules. The water vapour molecules enter or leave the polymer until equilibrium is reached. The capacitance of the polymer changes according to the amount of absorbed water in the polymer layer.

3.3. Diffusion and convection of humid air

In a gas mixture such as humid air, diffusion occurs spontaneously to establish uniformity of the system, where the diffusing substance (water vapour) moves in the direction of decreasing concentration. For a review of diffusion in the context of drying of porous media, see e.g. (Xu et al., 2020). The diffusion process very often takes place simultaneously with convection. In the case relevant to CUI, convection is driven by buoyancy, as hot and humid air is lighter than cold and dry air. A buoyancy driven flow caused by both density differences due to temperature variations and concentration variations is called double-diffusive convection, which is relevant in many engineering applications, including humidity migration in porous media (Trevisan and Bejan, 1985). The particular case of double-diffusive convection where the heat gradient is imposed horizontally and the concentration gradient vertically has received some attention in the literature (Mohamad and Bennacer, 2001).

The experimental setup in this work features a (predominantly) vertical gradient in water vapour concentration, with high concentration at the bottom near the water addition reservoir, and low concentration at the top. The setup also features a horizontal temperature gradient, with high temperature at the pipe wall (70°C) and low temperature at the cladding (ambient laboratory conditions at approx. 20°C). The gradients are illustrated in Fig. 3. As illustrated in this figure, there will in general also be a concentration gradient radially. Due to the slender aspect ratio of the insulation cross-section in the experimental setup, the radial gradient will be smaller than the vertical gradient.

For the present system it is of interest to estimate the relative importance of convection versus diffusion. When convection of the fluid occurs inside a porous medium, the convective velocity follows from Darcy's law, and the modified Rayleigh-Darcy number Ra can be used to characterize the ratio between transport due to thermal diffusion and transport due to convection. It is given by

$$Ra = \frac{g\beta\Delta T L\rho}{\alpha P_{yy}} \approx 0.4, \tag{10}$$

where the parameters that characterize the experimental setup in this work are: $g = 9.81 m/s^2$ acceleration due to gravity, $\beta = 3 \times 10^{-3} K^{-1}$ thermal expansion coefficient of air, $\Delta T = 50K$ temperature difference, $L = 0.06m$ radial thickness, $\alpha = 25 \times 10^{-6} m^2/s$ thermal diffusivity, $\nu = 22 \times 10^{-6} m^2/s$ kinematic viscosity, $P_{yy} = 9kPas/m^2$ is the vertical hydraulic resistivity. After the transformation using the expression for permeability of the mineral wool $k = \upsilon\eta\Delta x/\Delta P$, and hydraulic resistivity $P_{yy} = \Delta P/\upsilon L$, the obtained approximate value of 0.4 can be found.

The obtained value of the modified Rayleigh-Darcy number, $Ra \approx 0.4$, shows that some convective transport occurs, but the diffusive transport is a stronger effect in the present system. A detailed measurement of the convective transport could be obtained by the vertical temperature variation in the system. Qualitatively this can bee seen in the experimentally measured temperatures, but the uncertainty associated with the exact radial position of the temperature sensors in the strong temperature gradient, means that a quantitative estimate cannot be given with the present data. It may be possible to achieve this in future experiments by using significantly smaller and more accurate sensors.

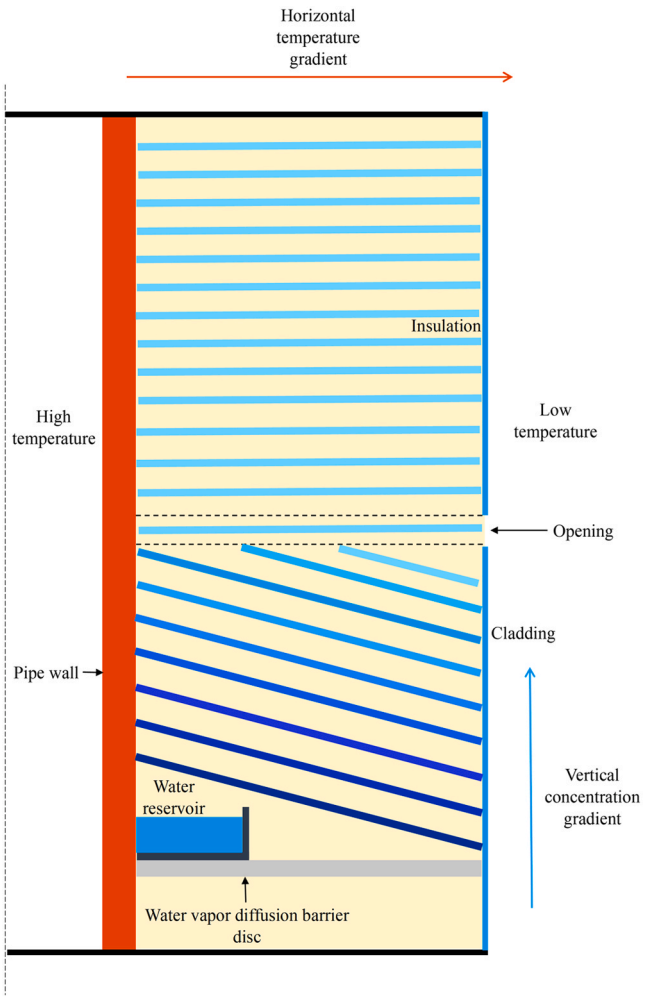

Fig. 3. Schematic illustration of the specific humidity (concentration) and temperature gradients during the transient drying process. The lines indicating constant specific humidity are generally sloped in the region where drying is occurring.

3.4. Mollier diagram for humid air in insulation systems

A common way to explain the processes related to thermodynamics of humid air is to use a Mollier diagram, which provides relationships between dry bulb temperature, relative humidity and specific humidity values. For the relevant thermodynamic states of humid air within the insulation material, a Mollier diagram is shown in Fig. 4. Three different cases for the radial distribution of humid air are shown. These are given as lines showing the variation in the specific humidity on the horizontal axis, while the temperature gradient between the hot pipe and cold cladding corresponds to the dry bulb temperature shown on the vertical axis. These cases correspond qualitatively to different positions in the vertical pipe experiments, where case 1 is encountered close to the opening to ambient, case 3 occurs close to the water reservoir, and case 2 is found between these two. Transport of humidity by diffusion will occur both along the coloured lines, thus changing their slopes, and between the regions represented by these lines, thus shifting the lines marked 2 and 3 towards line 1. *We emphasize that the cases 2 and 3 are drawn with straight lines for simplicity, in general they will be curved paths when the system is not in equilibrium.*

In Fig. 4 we have illustrated three possible situations for the *radial* variation in the humid air state. These cases are relevant for the

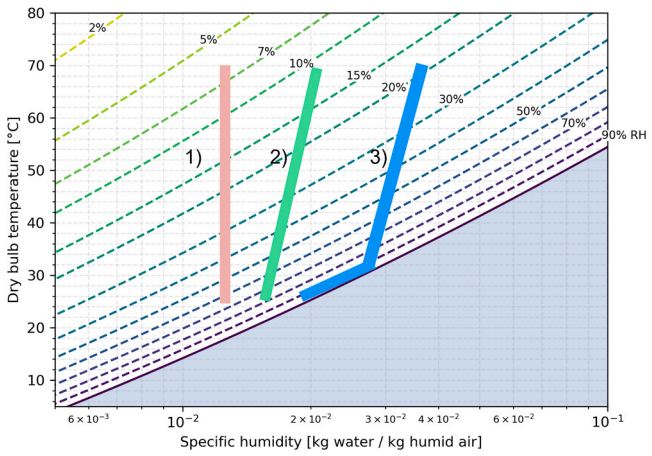

Fig. 4. Mollier diagram for humid air. The three coloured lines indicate three qualitatively different cases for the distribution of humidity along the temperature gradient in the insulation. In all cases it is assumed that we have a pipe temperature of 70°C, and a cladding temperature of 25°C. In case 1), there is diffusive equilibrium along the temperature gradient; in case 2), there is diffusion of moisture towards the cold cladding; in case 3), there is diffusion towards the cold side and condensation occurs, both at the cladding and a certain distance inside the insulation in the temperature range where the blue line follows the 100 % RH line.

evaporation and drying of the insulation system, and are described below.

1. Specific humidity is constant at the equilibrium concentration. There is no net diffusion taking place radially in the insulation, and the system is generally dry.
2. Specific humidity is higher at the hot surface, and diffusion takes place radially towards the cold surface. This situation occurs transiently after some water has entered near the hot surface. After some time, the system will reach an equilibrium state with constant specific humidity.
3. Similarly to case 2, this shows a transient situation with higher specific humidity at the hot surface driving diffusion towards the cold surface. Here the humid air reaches the point of condensation, and there is a kink in the blue line indicating that the specific humidity cannot exceed the value of saturated air at the given temperatures. Condensation will occur along the part of the blue line that follows the 100 % RH line. The distribution of liquid water along this section can not be trivially obtained.

3.5. Estimation of drying times based on diffusive flux approximations from the sensor data

In this section, we present a simple model to estimate the dry-out time of the insulation system, based on vertical diffusion from the reservoir to the opening. The diffusive flux for species i in multi-component systems with non-uniform density can be computed via the Fickian diffusion approximation

$$\boldsymbol{j}_i \approx -\rho D_i \nabla Y_i, \tag{11}$$

where D_i is an effective binary species diffusion coefficient. In diffusive equilibrium, the mass fraction is constant. For the binary water vapour-air system at hand, this corresponds to constant values of specific humidity. We assume that upon filling of the water reservoir, the humid air above the water interface is saturated. We further assume that gradients in specific humidity are only present up to the vertical height of the opening to ambient. The idealized situation in terms of specific humidity contours, is visualized in Fig. 3. The dry-out time of the reservoir can then be computed by estimating the mass-flux through the annular disk just above the water reservoir, assuming that the mass fraction gradient can be estimated by the saturated conditions at the reservoir side, and by the mass fraction values obtained from the sensor just above, on the insulation side. Similarly, the vertical mass flux across the annular disks at the height of the opening, and corresponding to sensor layer one, two, and three, can be estimated by values for mass fraction provided by the sensors closest to the opening height in layer one, two and three, and the assumption of constant specific humidity (equal to ambient conditions) at the height of the opening. Integrating the mass fluxes over the bounding areas, provides the mass flow rate out of the enclosed volumes. By conservation of mass, the mass flow rate is also given by the amount of added water to the system, divided by the (unknown) transport time-scale. The diffusive time scale for transport of water vapour out of the reservoir volume enclosed by the surface A_{res} is then given by

$$t_{\text{res}}^{\text{diff}} = -\frac{M_{\text{add}}}{\rho_{\text{res}} D_{\text{res}} A_{\text{res}} (\partial Y_{\text{w}}/\partial z)_{\text{res}}}, \tag{12}$$

where M_{add} is the amount of water added to the reservoir, and subscripts $_{\text{res}}$ denote evaluation of the respective quantity at the reservoir conditions. The mass fraction gradient is evaluated from sensor readings obtained at the sensor just above the reservoir, and the assumed saturated reservoir conditions. Equivalently, the diffusive dry-out time for the insulation volume bounded by the water reservoir and the opening to ambient, is given by

$$t_{\text{amb}}^{\text{diff}} = -\frac{M_{\text{add}}}{\sum_k \rho_k D_k A_k (\partial Y_{\text{w}}/\partial z)_k}, \tag{13}$$

where $k = 1, 2, 3$ denotes the (radial) sensor layer, where the quantities are evaluated. In Eq. (13), the mass fraction gradient is evaluated from sensor readings obtained at the sensors from the three sensor layers closest to the opening, i.e., approximately at the vertical position of the opening, and the assumed constant ambient state. An illustration of the bounding volumes is given in Fig. 5.

To evaluate the quantities occurring in Eq. (12) and Eq. (13), we employ a commonly used correlation for the diffusion coefficient's dependency on temperature Nellis and Klein (2020)),

$$D(T) = D_0 \left(\frac{T}{T_0}\right)^{1.685}. \tag{14}$$

Specific humidities are obtained from relative humidity and temperature readings from the sensors and the known (saturated) state of the near-water reservoir as well as the ambient conditions. The diffusive model is applied to sensor data in Section 5.

4. Experimental methods

4.1. Description of the vertical setup configuration

The measurement of relative humidity and temperature inside the insulation was performed using the sensor configuration and the experimental setup shown in Fig. 6. A logging system with multiplexers (Omega, OM-240) was used to record the output data from analogue temperature and relative humidity sensors (Michell Instruments PCMini52, Driesen en Kern, DKRF4001). A vertical steel pipe with inner and outer radius of 94 mm and 104 mm was used. The pipe can be heated up to 70°C using a thermostatically controlled electric heating cable mounted at the inside of the pipe. A secondary thermal safety control was used for shutting down the heating system if the temperature exceeded 80°C. An annular water reservoir made from plastic was positioned in contact with the pipe at vertical position 170 mm as measured from the base of the pipe. The reservoir has a height of 30 mm and wall thickness of 2 mm. The reservoir can contain 335 mL of water, and is connected to two pieces of tubing for filling.

A hydrophobic mineral wool insulation (Rockwool PS 960) has been

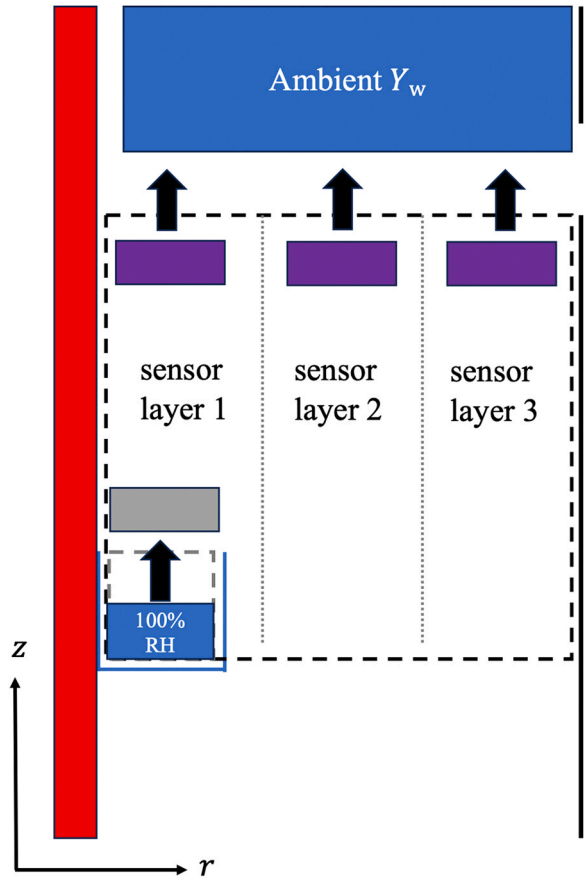

Fig. 5. Vertical cross section of the bounding volumes considered in the diffusive model. The hot pipe is represented by the red shaded area on the left, and the cladding is illustrated by the black vertical line to the right. Black arrows denote the vertical component of the diffusive flux vectors. Gradients in specific humidity are evaluated from assumed known quantities (reservoir state, constant specific humidity above the opening in the cladding) and from the measurements of the indicated sensors, respectively. The small box enclosing the water reservoir is used to calculate t_1^{diff}, and the large box (subdivided in sensor layers), is used to calculate t_2^{diff}, as explained in the text.

used and assembled in two *insulation layers*, both with 30 mm thickness, as indicated by the dashed line in Fig. 6 (b). The insulation is covered by a rigid metallic cladding which is painted black, cf. Fig. 6 (a). A circumferential ventilation opening of height 40 mm is present in the cladding. The vertical position of the opening is at 410 mm from the bottom of the pipe.

Sensors are placed at different vertical and radial positions in the insulation material, as shown in Fig. 6 (b). In the following we distinguish the three *sensor layers*: The first layer of sensors is placed next to the inner pipe, and covered by the first insulation layer. Sensors placed in the second sensor layer are positioned in small pockets that were made on the outside of the first insulation layer. Sensors in the third sensor layer are located in pockets on the outside of the second insulation layer. According to this arrangement, the corresponding radial distances of the sensor layers from the inner pipe are 0 mm (sensor layer 1), 30 mm (sensor layer 2) and 60 mm (sensor layer 3), respectively. There are 8 sensors in sensor layer 1, and 7 sensors in sensor layer 2 and 3, cf. Fig. 6 (b). In addition, a reference sensor is providing the lab environment. One sensor is fixed to the outside of the cladding just above the opening, and one sensor is placed below the water barrier plastic disc below the reservoir. This plastic disc is installed to prevent liquid water, originating from condensation at the cladding, from running down along the inner side of the cladding and collecting at the bottom. The disc has a tight fit against the cladding, but was not expected to be completely diffusion tight.

4.2. Calibration of the sensors

A climate chamber (Weiss SB2/300/40) was used to calibrate the sensors before the experiments. Calibration of the sensors for relative humidity and temperature was performed for the expected range of temperatures and humidities in the experiments, i.e., between 10 % and 95 % relative humidity, and between 15 and 70°C. Linear calibration curves were found for each sensor and are used in the subsequent experimental measurements.

4.3. Experimental procedure

Before the liquid water was introduced, the pipe was heated up to 70°C until an approximate equilibrium with the ambient had been reached. Typically this equilibration time was at least 24 h. When the pipe wall temperature reached the set value, water at approximately 68°C was introduced through a 3 mm inlet pipe into the water reservoir using a 50 mL syringe in several batches. The inlet pipe was then closed to prevent transport of water vapour through any other paths than the circumferential ventilation opening.

Evaporation of water from the reservoir starts immediately after water addition, and changes in temperature and relative humidity values were monitored. Pipe wall temperature and the amount of liquid water introduced in the water reservoir were controllable factors in the experiment, while fluctuations of ambient temperature and relative humidity in the laboratory were uncontrollable parameters. After the experiment had been completed, the data were collected from the data-logger and analysed.

4.4. Experimental uncertainty

No measurement system is perfect, and the error of a measurement is defined as the difference between the measured value and the true value of the measurement. In the present experiment there are several potential sources of errors and uncertainties, which we summarize here.

First of all, there is the uncertainty in the measurements themselves. An overview of the uncertainty specified from the sensor manufacturers is presented in Table 1.

The relative humidity values provided by the sensors is given by a correlation programmed into the microcontroller of the sensing device. The correlation is a function of temperature and capacitance (i.e. the mass of absorbed water). Thus, it is necessary for the humidity sensor to also measure temperature, and the measurement uncertainty in temperature propagates non-linearly into the relative humidity uncertainty. For this reason, accurate relative humidity sensors need to incorporate very accurate temperature measurements. To be specific, the contribution of the temperature uncertainty into the relative humidity uncertainty is given by

$$\delta(RH) \approx RH\left(\frac{\mathrm{d}}{\mathrm{d}T}\log p_{\mathrm{sat}}\right)\delta T. \tag{15}$$

The uncertainty in the relative humidity is thus on the order of 2 %-points for a $\delta T \approx 0.2$ K, for the range of temperatures and relative humidities at hand, as given by the sensor manufacturer and discussed in Section 4.4. The uncertainty in the absolute humidity due to uncertainty in the relative humidity temperature measurements can be found by Gaussian error propagation, which for the conditions at hand gives $\delta(AH) \approx 0.4\ \mathrm{g\,m^{-3}}$ at ambient/cladding conditions, and $\delta(AH) \approx 4\ \mathrm{g\,m^{-3}}$ at the hot pipe wall.

Assuming a constant temperature uncertainty of $\delta T \approx 0.2$ K and propagating the error through the expression for specific humidity, gives a relative uncertainty in the range of 1.7–2.5 % and an absolute uncertainty of ca $5 \times 10^{-4}\ \mathrm{kg\,kg^{-1}}$, respectively. If the measurand varies in

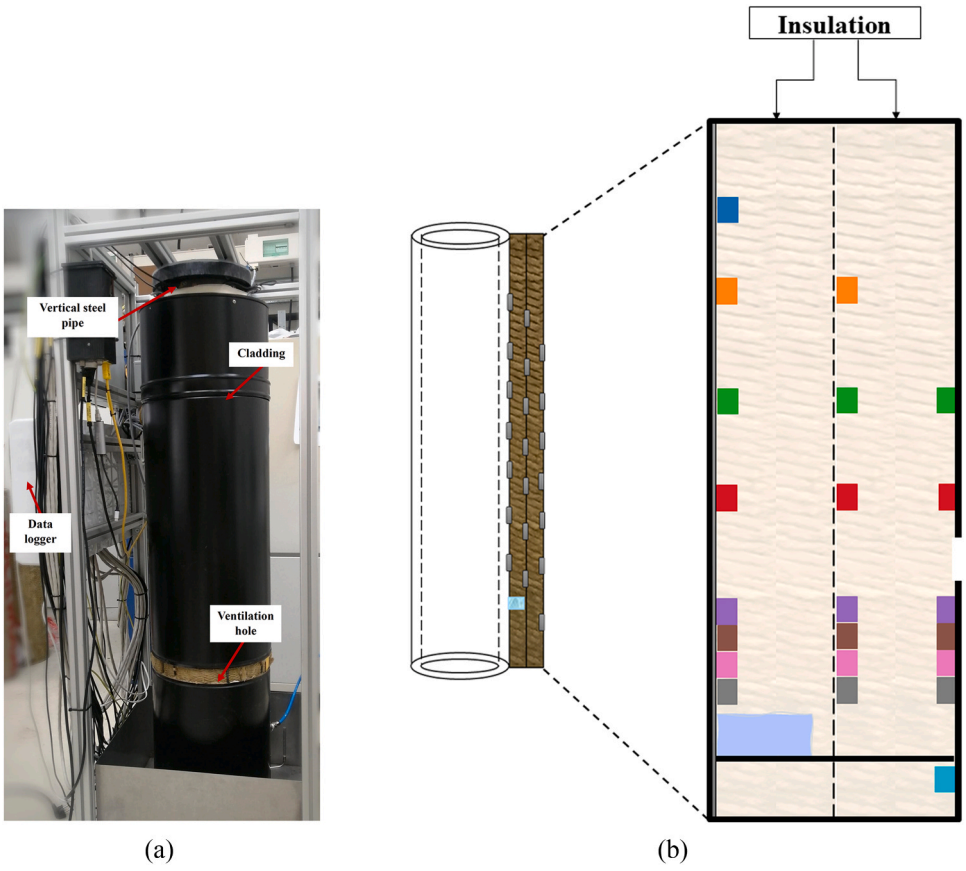

Fig. 6. (a) Photograph of the instrumented vertical pipe, and (b) schematic of the sensor layout.

Table 1
Uncertainty of the sensors specified in the datasheet from sensor manufacturers.

Sensor type	Sensor output	Accuracy	Range
PCMini	RH	± 2 %	[0, 100]%
	T	± 0. 2°C	[− 20, 80°C]
DKRF4001	RH	± 2 %	10–90 %
	RH	± 3.5 %	> 90 % or < 10 %
	T	± 0.6– ± 2. 6°C	[− 20, 80°C]

a spatial region there will be the spatial error. The sensors in the first sensor layer are placed next to the pipe wall. However, it is difficult to say with certainty that all the sensors have similar thermal contact with the pipe wall. Considering the strong temperature gradient that exists, from 70°C on the pipe wall to ≈ 25°C on the cladding across a distance of 6 cm, a 1 mm difference in the radial sensor position gives a 0.75°C difference. Fig. 7 shows the scatter in temperature values in the first sensor layer. Note how the evaporation of water leads to a temperature drop in the sensors located between the reservoir and the opening height. The observed scatter can be caused both by positional uncertainty, by uncertainty in the sensors, and by convection, as discussed in Section 3.3. With the present sensors, it is not possible to distinguish these effects with certainty.

Regarding the injected water volume, the water was introduced through the inlet pipe into the water reservoir, using a syringe with maximum volume of 50 mL. The measuring of water volume in the syringe gives rise to readability error. The estimated error due to readability is $\pm$ 0.5mL.

To prevent the presence of escape paths for water vapour different than the circumferential opening, the cladding was sealed tightly and furthermore covered with several layers of tape. Below the reservoir, the disc was not perfectly sealed against water vapour, but has removed

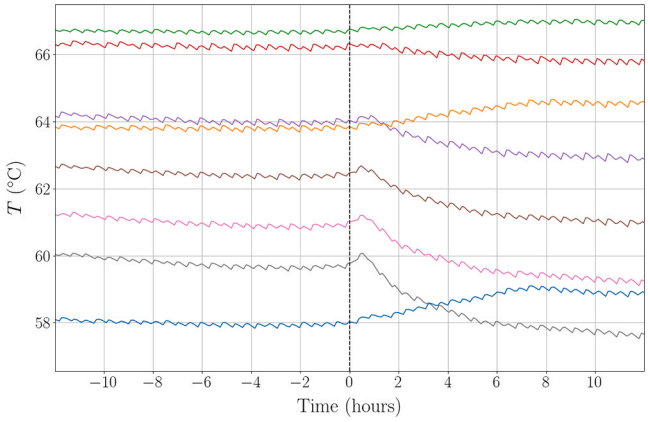

Fig. 7. Temperature values in the first layer, rolling mean using 5 samples. The dashed line indicates the water addition event. Colours are according to the schematic in Fig. 6b.

uncertainty regarding liquid water accumulating at the bottom of the system. The readings of the sensor placed below the plastic disc confirmed that this space became dry at the same time as other sensors returned to the dry state.

Electrical noise is one of the common environmental causes of random error. In this experimental system, the temperature controller has been causing scatter in the temperature reading due to heating switching on and off. This caused temperature fluctuations of ± 1°C around the set-point.

5. Results

The results of the different water addition experiments are presented in this section. To analyse the drying dynamics of the mineral wool insulation material, four different cases of controlled water addition are investigated. We perform addition of 250 mL, 125 mL, 63 mL water to the reservoir, in addition to a double addition of 250 mL of water.

The plots shown in the following sub sections are the rolling-mean averaged measurements of temperature and humidity over time. As described in the previous section, the sensors are mounted in groups at three different radial positions, and we refer to these as the first (inner) layer of sensors, the second (middle) layer of sensors, and the third (outer) layer of sensors.

As discussed in Section 3.3, the specific humidity Y_w enters into the diffusion equation. Hence, the specific humidity is presented in the following plots, calculated according to Eq. (9). Considering specific humidity has several benefits over considering the measured relative humidity values, including straight-forward comparison of values between the three layers, as well as removing to a large extent the effect of the radial position uncertainty which makes it difficult to directly compare relative humidity values within each layer.

Time evolutions for specific humidity and temperature are shown for the 250 mL single and double water addition experiments. Results from the 125 mL and 63 mL experiments are deferred to the Appendix for better readability. These experiments have been analysed in the same fashion as the 250 mL water additions cases presented here, and the resulting drying times are included in the Fig. 15.

5.1. Addition of 250 mL liquid water

Figs. 8, 9, 10 show the measurements from the test with addition of 250 mL liquid water. The pipe was kept at a temperature of 70°C throughout the experiment. The water addition event is marked by a vertical dashed line. When evaporation of water starts due to heating of the water in the reservoir, the specific humidity shows a sharp increase. Elevated and approximately constant values can be observed for around 29 h. Then, a sharp decrease occurs. This drop is associated with the dry out of the reservoir. Subsequently, we refer to the period between the time of water addition, and the sharp decrease in specific humidity of all sensors, as the first drying time. The first drying time corresponds to the time of wetness of the insulated equipment. The second period of drying is characterized by a gradual decrease in the specific humidity, and lasts for approximately 120 h. The second drying time corresponds to the dry out of the insulation. Both observed drying times are identical for the three sensor layers.

In the data from the first sensor layer, there is also a clear

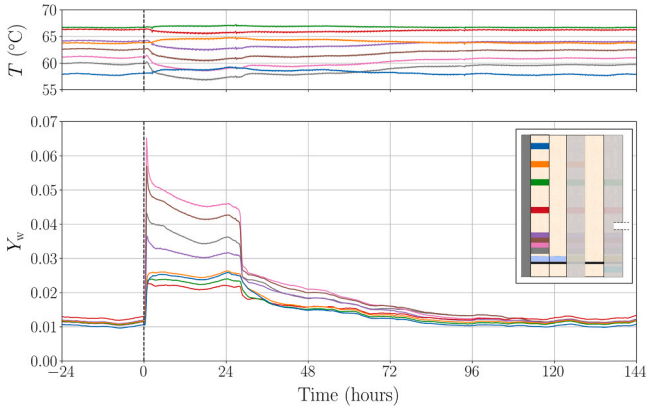

Fig. 8. Temperature and specific humidity response in the first sensor layer during the addition of 250 mL of liquid water. The specific humidity Y_w is calculated according to Eq. (9).

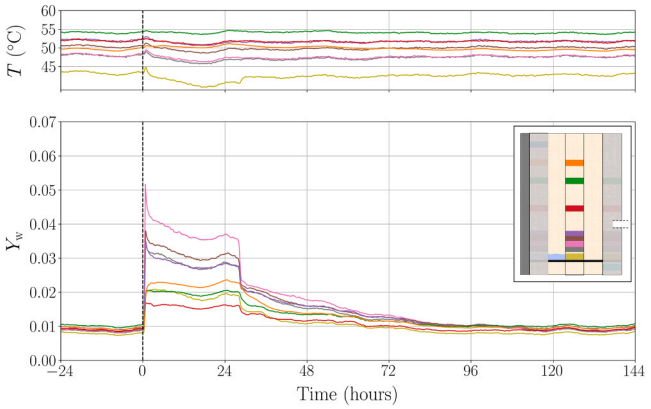

Fig. 9. Temperature and specific humidity response in the second sensor layer during the addition of 250 mL of liquid water. The specific humidity Y_w is calculated according to Eq. (9).

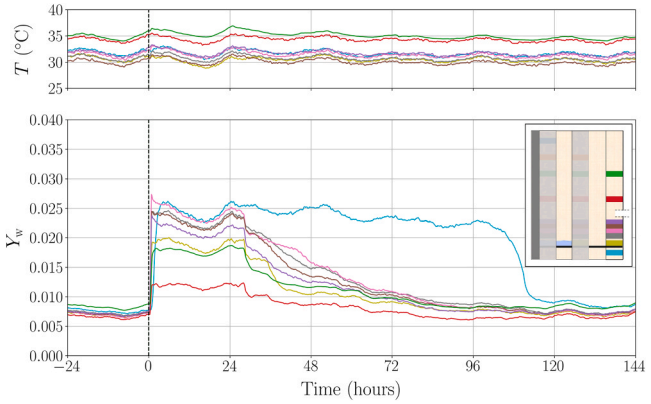

Fig. 10. Temperature and specific humidity response in the third sensor layer during the addition of 250 mL of liquid water. The specific humidity Y_w is calculated according to Eq. (9).

temperature drop[1] following the water addition. This is associated with the phase transition of liquid water to water vapour, consuming energy equal to the latent heat of evaporation, and leading to decrease in temperature for the extend of the evaporation period. When the primary drying process has completed, the temperatures all return to their initial values. Note also that the sensors in the third layer are somewhat affected by the day-night cycles in the laboratory, cf. Fig. 10, while the inner layer is not affected (Fig. 8).

Drying times have been estimated as illustrated in Fig. 11: For each sensor we subtract the specific humidity one day prior to water addition, and thereby construct the excess specific humidity with respect to the sensors' initial value. The excess specific humidity is then average over the 24 h before the water addition. This processing results in smooth curves that represent the deviation in specific humidity in response to the water addition, and eases comparison of readings obtained at different sensor positions. The first drying time is found when the sensors simultaneously show a significant drop in excess specific humidity (marked by the second dashed line, with the first drying time denoted by t_1^{obs}). The second drying time is found when the excess specific humidity of the sensors coincide again (marked by the third dashed line and denoted by t_2^{obs}). As illustrated by the gray shaded area in Fig. 11, there is

[1] Most sensors show a temperature drop, but the sensors mounted near the top show a small temperature increase, due to the thermostat adding the same amount of heat along the whole pipe height.

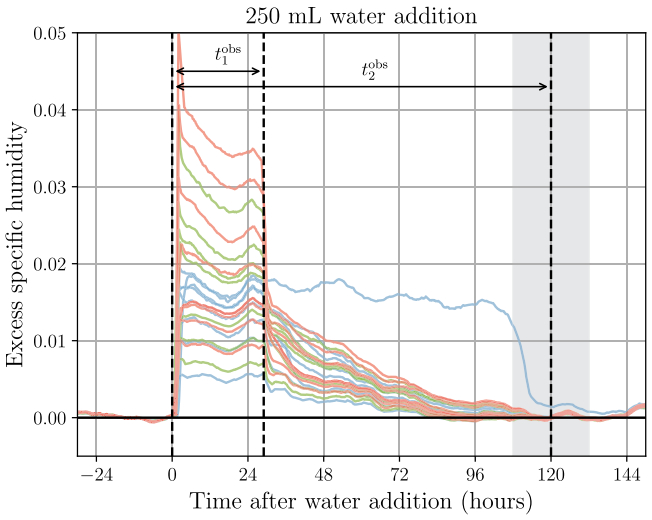

Fig. 11. Excess specific humidity above each sensors' baseline specific humidity (averaged over one day before water addition) for all sensor layers as function of elapsed time after water addition: Layer one (orange), layer two (green), and layer three (blue). The dashed vertical lines indicate the water addition event at zero hours, the first drying time, t_1^{obs}, at 29 h, and the second drying time, t_2^{obs}, at 120 h, respectively. The grey shaded area shows the uncertainty range in the second drying time.

some uncertainty connected to this visual measure. Another option to assess the second drying time, is to consider the second significant drop in humidity for the sensor positioned below the water barrier disk (cf. Fig. 10). However, estimating the second drying time based solely on the readings from one single sensor is deemed as less robust than considering the collective return to equilibrium of all sensors. Nonetheless, the fact that the sensor below the disk returns to the dry state at a similar time as the sensors placed above the disk, indicates that there is no significant liquid water accumulation due to condensation below the disk.

5.2. Repeated addition of liquid water

The double addition of water experiment was started from the dry state at 70˚C before introduction of 250 mL water. The sensor signals were monitored during the primary drying phase, and upon observation of the sharp drop in humidity that indicates the end of first drying state, another injection of 250 mL water was performed.

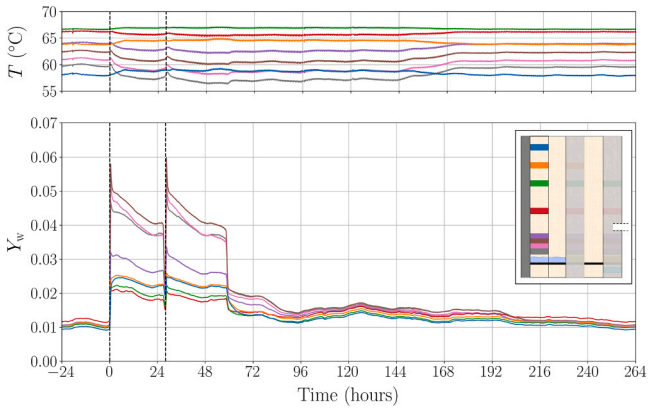

Fig. 12. Temperature profile and specific humidity response to the introduction of water as a function of time for the first sensors layer. The different colours of the line represent sensor at different position within first sensor layer, on the pipe surface.

The observed humidity and temperature signals in the different sensor layers are shown in Figs. 12, 13, 14. It is clearly seen that the humidity response to the second addition of water is very similar to the first addition. Note that upon re-addition of water, the specific humidity values are stabilizing at approximately the same value as the first addition. The first drying times are equal, and observed to be close to 30 h, as expected from the single 250 mL water addition. This indicates that the first drying period is not influenced by the residual amount of water vapour residing in the insulation, and only depends on the reservoir conditions. The second drying time, measured for the second water addition, is approximately 174 h, about $\sqrt{2}$ longer than the 120 h measured for the single 250 mL addition experiment, highlighting the complex interaction between the physical processes in place.

5.3. Estimation of drying times

Here, we apply the simple vertical diffusive model suggested in Section 3.5 to the sensor data obtained from the 63 mL, 125 mL, and 250 mL experiments. Calculated values from the diffusive flux model or the first drying-time (reservoir dry-out time) and the second drying time (insulation dry-out) are denoted t_1^{diff} and t_2^{diff}, respectively. Steadiness of diffusive fluxes in the volume between the reservoir and the opening should provide similar estimates for the first drying time, when evaluating the diffusive fluxes in the near reservoir vicinity (Eq. (12)) and close to the opening (Eq. (13)). To estimate the reservoir dry-out time, we assume that the humid gas in the void space between the water surface and the bottom part of the insulation is at saturation, and at the water temperature of 70˚C. The vertical diffusive flux is estimated via the sensor readings at a position located 50 mm above the reservoir when using Eq. (12). We use the plateau values for the first peak in the specific humidity signals. When using Eq. (13), the sensors located in sensor layer 1, 2, and 3, at a position 200 mm above the reservoir are used, and gradients are evaluated towards the assumed constant ambient specific humidity. The calculated dry-out times are listed and compared against the observed dry-out times in Table 2. We see that the dry-out times of the water reservoir computed via the diffusive model and sensor data close to the reservoir, agrees with the observed dry-out times to within 21 %, whence evaluation of the diffusive fluxes close to the opening over-estimates the reservoir dry-out by almost a factor of three. This deviation indicates that during the first drying phase, processes other than diffusion affect the mass fraction field. The secondary dry-out time, or insulation dry-out time, is computed based on the mean value of the specific humidity just after the reservoir has dried out, and the base value, i.e., we assume a linear decrease in specific humidity from the levels at the onset of insulation drying, to the base level, when the insulation is back at the humidity state it was at before water was added to the reservoir. As for the first drying time, the vertical gradient

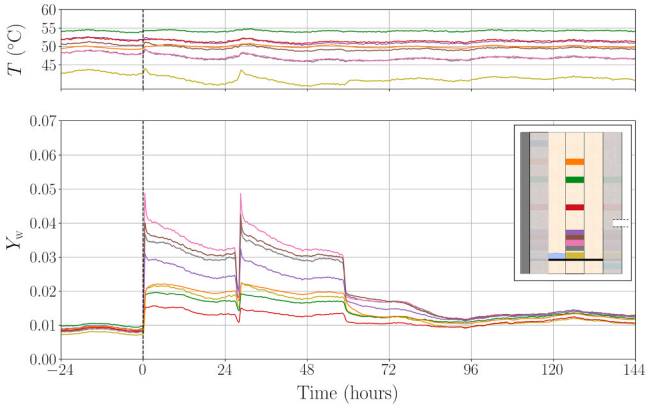

Fig. 13. Temperature profile and specific humidity response to the introduction of water as a function of time for the second sensors layer.

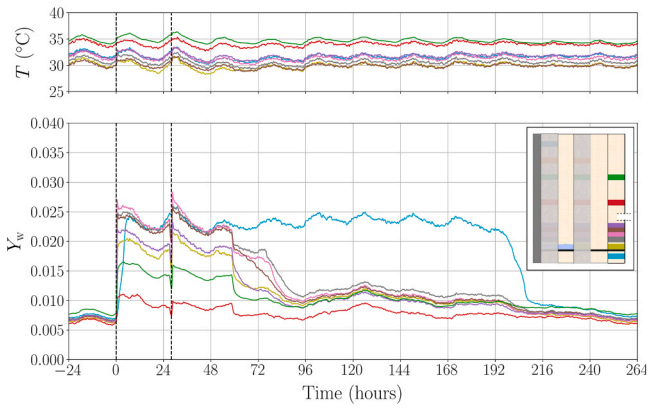

Fig. 14. Temperature profile and specific humidity response to the introduction of water as a function of time for the third sensors layer.

Table 2
Estimation of the water reservoir dry-out time using the vertical diffusive flux model based on the sensor closest to the reservoir (top half) and sensors close to the cladding opening (bottom half).

M_{add} [mL]	t_1^{diff} [h]	t_1^{obs} [h]	t_1^{diff}/t_1^{obs}	Sensor position
63	8.8	8.6	1.02	Near reservoir – Eq. (12)
125	17.5	15.0	1.17	
250	35.0	29.0	1.21	
63	21.6	8.6	2.51	Near opening – Eq. (13)
125	44.3	15.0	2.95	
250	83.5	29.0	2.88	

in mass fraction for each sensor layer in Eq. (13) is computed with respect to the (assumed constant) ambient value for specific humidity at the three radial coordinates, respectively. The calculated drying times are listed in Table 3. The agreement for the insulation dry-out time calculated with the diffusive model is up to 20 %, compared to the observed insulation dry-out times.

6. Discussion

As discussed previously there is a multitude of physical effects that interact in the experiments reported here. Water vapour is produced by evaporation of liquid water from the water reservoir, and transported by diffusion from higher values of specific humidity to lower values, i.e., from the reservoir towards the opening to ambient. Convection due to buoyancy differences in the air caused by the radial temperature gradient cause a slow circulation that increases the transport of humid air from the hot pipe towards the colder cladding. Adsorption/desorption of water between the fibres and the gas phase means that a significant amount of water can be stored in the bulk, interacting with the diffusion process. Condensation can occur both inside the insulation and at the cladding when saturated hot air diffuses into the colder regions, and subsequently there will be evaporation during the drying of the system.

Several interesting points from the specific humidity curves and observed drying times can be noted. Firstly, we note that there is a linear relation between added water amount and first drying time, i.e., reservoir dry-out time. This can be understood in terms of the initial evaporation process which features a linear relationship between evaporated mass and dry-out time, as the imposed heat flux from the pipe surface into the reservoir (and the insulation) is nearly constant. In Section 3.5 we suggested a simple vertical diffusive flux model, showing that the first drying time can also be estimated by measuring the amount of water vapour that is transported past the sensor just above the water reservoir. The diffusive transport from the saturated water reservoir to the nearest sensor is linear in the amount of added water.

Comparing the three sets of experiments, it is seen that the recorded specific humidity is strikingly equal for the first drying period. In particular, the values of specific humidity during the first drying period, as well as the recorded values immediately after the sharp drop at the onset of the second drying period, are very similar. Hence, for all experiments, the *gas phase* in the insulation is in a comparable state during and just after evaporation from the reservoir, and similar second drying times should be expected if only diffusion from the reservoir to the opening were the dominant mechanism. The increase in evaporation time for more added water, also means that there is more time for convection to bring high humidity air towards the cladding, for adsorption to take place on the fibres, and for condensation in the bulk and on the cladding to occur.

Equilibrium adsorption is related to the local humidity state, and should therefore be similar during the first drying time for the three experiments, as the humidity distributions are very similar. Measurements of the adsorption isotherm for ProRox PS960 at 40°C show that the equilibration time scale is on the order of tens of hours, i.e., the adsorption is likely *not* proceeding at equilibrium, and more liquid water can be adsorbed onto the fibres when exposed to prolonged supply of water vapour. When the supply of humid air to the cladding ceases, this excess liquid water is evaporating into the gas phase again, increasing the second drying time, meaning that more added water to the reservoir, prolongs the second drying time, consistent with the observations from Fig. 15. The second drying times appear to scale non-linearly with the added water mass, but unravelling the exact functional dependence will require additional experiments, preferably with even higher accuracy provided by latest-generation sensors. From the double water addition experiment, cf. Fig. 14, we find similar first drying times for the consecutive water additions, whence the second drying time is approximately a factor of $\sqrt{2}$ longer than the second drying time for the single 250 mL water addition event. The observations listed above point towards a complex interaction of diffusion, adsorption, convection and condensation/evaporation leading to redistribution of the added water

Table 3
Estimation of the insulation dry-out time based on the vertical diffusive flux model using sensors close to the cladding opening.

M_{add} [mL]	t_2^{diff} [h]	t_2^{obs} [h]	t_2^{diff}/t_2^{obs}
63	35.3	38	0.93
125	80.0	92	0.87
250	147.9	120	1.23

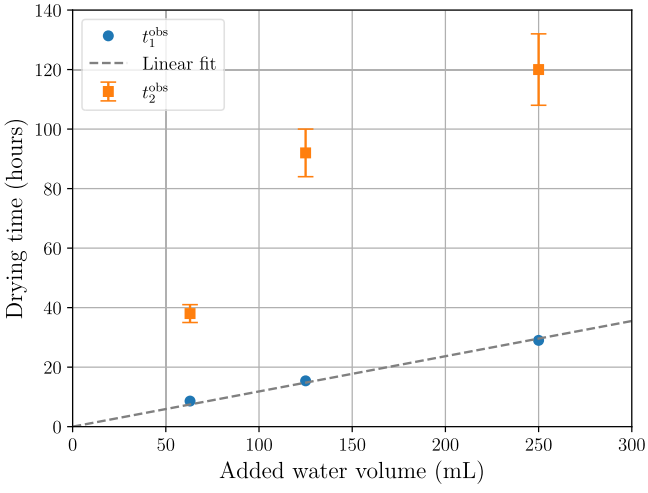

Fig. 15. Overview of the observed first and second drying times in relation to the amount of added water. Error bars on the second drying time are calculated as illustrated in Fig. 11.

mass in the system. The overall drying time for the added water to leave the system, however, is consistent with a scaling proportional to the square root of added water mass, a typical signature of diffusion controlled systems.

7. Conclusion

We have performed experiments on liquid water addition to an insulated vertical hot pipe. Two characteristic drying regimes are identified, associated with evaporation of liquid water from the water reservoir until reservoir dry-out, followed by insulation drying. In the context of understanding and preventing corrosion under insulation, these two regimes are associated with the time of wetness of the equipment, and the time where humidity sensors would give elevated readings, respectively. We have shown that the first drying time scales linearly with added water mass, given that the evaporation process for a constant heat flux, as well as diffusive transport at the centimetre scale near the reservoir, is linear in the added water mass. The second drying mode is affected by all physical phenomena at hand: diffusion, convection, adsorption/desorption, condensation/evaporation at the cladding.

Adding different amounts of water yields similar responses of the gas phase humidity peak values during the first drying period, with differences between experiments only pronounced in the length of the first drying stage. As a similar humidity distribution at the end of the primary drying will lead to similar diffusive fluxes, the explanation for the prolonged second drying time for larger amounts of added water is associated with the time-integrated effects caused by convection, adsorption/desorption and condensation/evaporation. The overall system drying dynamics observed in the presented experiments can be described by a square root dependence of the added water mass, giving an overall diffusion-like characteristic.

The findings in this work confirm that humidity and temperature monitoring of insulated process equipment indeed is a promising solution to quantify water ingress. A simple diffusive flux model provides good agreement for the insulation drying time, and can be computed from sensors close to the cladding opening. The water reservoir drying time, i.e., the *time of wetness*, calculated by the diffusive model using the readings provided by the near-cladding sensors, is overestimated significantly. In terms of a sensor monitoring solution to detect water in the insulation system, further work is needed to understand the connection between evaporation at the equipment surface and the resulting sensor humidity responses.

In practical terms, the findings indicate that monitoring the insulation wetness (the second drying time) provides a conservative estimate of the time-of-wetness, which again determines the corrosion rate. However, the exact relation between the first and second drying times will depend on the specific design of the system, including insulation and cladding design, ambient climate, and pipe temperature. The present work constitutes the first openly available study which demonstrates the viability of monitoring CUI implicitly via detecting the humidity in the insulation system. The findings in this work are also of relevance for improving the design of insulation and cladding systems to minimize the impact of corrosion under insulation. Further work should be undertaken to investigate the performance of different cladding solutions and insulation systems, in light of the novel understanding of humidity dynamics that has been presented in this work.

CRediT authorship contribution statement

Daniela S. Damaceno: Data curation, Investigation, Methodology, Supervision, Visualization, Writing – review & editing. **Hristina Dragovic:** Investigation, Visualization, Writing – original draft. **Åsmund Ervik:** Conceptualization, Funding acquisition, Methodology, Project administration, Supervision, Writing – review & editing. **Ole H.H. Meyer:** Conceptualization, Funding acquisition, Formal analysis, Methodology, Software, Visualization, Writing – review & editing.

Declaration of Competing Interest

The authors declare the following financial interests/personal relationships which may be considered as potential competing interests: All authors report financial support was provided by Research Council of Norway, Equinor, Shell and Gassco.

Acknowledgements

The authors would like to thank colleagues S.T. Munkejord, M. Aa. Gjennestad, I. Hjorth and H. Deng at SINTEF, O.J. Nydal at NTNU, as well as M. Fransen and S. Terpstra at Shell, for fruitful discussions on these topics. This work was supported by the PredictCUI project coordinated by SINTEF Energy Research, and the authors gratefully acknowledge the contributions of Equinor, Gassco, Shell, and the PETROMAKS 2 programme of the Research Council of Norway (308770).

Appendix A. Supporting information

Supplementary data associated with this article can be found in the online version at doi:10.1016/j.psep.2024.08.016.

References

Anderson, S.A., 2010. Corrosion under insulation: out of sight, out of mind? Hydrocarb. Eng. 4.

Angani, C.S., Park, D.G., Kim, C.G., Leela, P., Kollu, P., Cheong, Y.M., 2010. The pulsed eddy current differential probe to detect a thickness variation in an insulated stainless steel. J. Nondestruct. Eval. 29, 248–252. https://doi.org/10.1007/s10921-010-0083-3.

Belleudy, C., Woloszyn, M., Chhay, M., Cosnier, M., 2016. A 2D model for coupled heat, air, and moisture transfer through porous media in contact with air channels. Int. J. Heat. Mass Transf. 95, 453–465. https://doi.org/10.1016/j.ijheatmasstransfer.2015.12.030. ⟨https://linkinghub.elsevier.com/retrieve/pii/S001793101501073X⟩.

Brett, C.R., Raad, J.A.d., 1996. Validation of a pulsed eddy current system for measuring wall thinning through insulation. SPIE 2947, Nondestruct. Eval. Uti. Pipelines 211–222. In: ⟨https://www.spiedigitallibrary.org/conference-proceedings-of-spie/2947/0000/Validation-of-a-pulsed-eddy-current-system-for-measuring-wall/10.1117/12.259169.full⟩, 10.1117/12.259169.

Brindley, J., Griffiths, J., Hafiz, N., McIntosh, A., Zhang, J., 1999. Criteria for autoignition of combustible fluids in insulation materials. Process Saf. Environ. Prot. 77, 61–68. https://doi.org/10.1205/095758299529811.

Buck, A.L., 1981. New equations for computing vapor pressure and enhancement factor. J. Appl. Meteorol. Climatol. 20, 1527–1532. https://doi.org/10.1175/1520-0450(1981)020<1527:NEFCVP>2.0.CO;2. ⟨https://journals.ametsoc.org/view/journals/apme/20/12/1520-0450_1981_020_1527_nefcvp_2_0_co_2.xml⟩.

Caines, S., Khan, F., Shirokoff, J., 2013. Analysis of pitting corrosion on steel under insulation in marine environments. J. Loss Prev. Process Ind. 26, 1466–1483. https://doi.org/10.1016/j.jlp.2013.09.010. ⟨https://www.sciencedirect.com/science/article/pii/S0950423013001873⟩.

Caines, S., Khan, F., Shirokoff, J., Qiu, W., 2015. Experimental design to study corrosion under insulation in harsh marine environments. J. Loss Prev. Process Ind. 33, 39–51. https://doi.org/10.1016/j.jlp.2014.10.014. ⟨https://www.sciencedirect.com/science/article/pii/S0950423014001739⟩.

Caines, S., Khan, F., Shirokoff, J., Qiu, W., 2017. Demonstration of increased corrosion activity for insulated pipe systems using a simplified electrochemical potential noise method. J. Loss Prev. Process Ind. 47, 189–202. https://doi.org/10.1016/j.jlp.2017.03.012. ⟨https://www.sciencedirect.com/science/article/pii/S0950423016303904⟩.

Cao, Q., Pojtanabuntoeng, T., Esmaily, M., Thomas, S., Brameld, M., Amer, A., Birbilis, N., 2022. A Review of Corrosion under Insulation: A Critical Issue in the Oil and Gas Industry. Metals 12, 561. https://doi.org/10.3390/met12040561. ⟨https://www.mdpi.com/2075-4701/12/4/561⟩. number: 4 Publisher: Multidisciplinary Digital Publishing Institute.

Cheng, W., 2012. Pulsed Eddy Current Testing of Carbon Steel Pipes' Wall-thinning Through Insulation and Cladding. J. Nondestruct. Eval. 31, 215–224. https://doi.org/10.1007/s10921-012-0137-9.

Clay, M., Kidd, M., Gale, A., Boardman, T., Murphy, J., Wynn, T., Naylor, S., Ellwood, J., 2020. Understanding loss of containment of non-radiological chemotoxic materials in the civil nuclear and process industries. Process Saf. Environ. Prot. 136, 203–213. https://doi.org/10.1016/j.psep.2019.11.042. ⟨https://www.sciencedirect.com/science/article/pii/S0957582019321378⟩.

De Vogelaere, F., 2009. Corrosion under insulation. Process Saf. Prog. 28, 30–35. https://doi.org/10.1002/prs.10276.

Dyrbøl, S., Svendsen, S., Elmroth, A., 2002. Experimental Investigation of the Effect of Natural Convection on Heat Transfer in Mineral Wool. J. Therm. Envel. Build. Sci. 26, 153–164. https://doi.org/10.1177/0075424202026002930.
Fitzgerald, B.J., Lazar, P., Kay, R.M., Winnik, S., 2003. Strategies to Prevent Corrosion Under Insulation in Petrochemical Industry Piping. In: NACE CORROSION 2003. OnePetro. In: ⟨https://onepetro.org/NACECORR/proceedings-abstract/CORR03/All-CORR03/114834⟩.
Fransen, M., Beekers, J., Terpstra, S. 2018. Corrosion under Insulation (CUI) Detection. Technical Report, Shell. Published in Research Disclosure RD652041.
Fu, J., Chen, G., Zheng, X., Gao, Q., Qiu, S., Xu, Z., 2021. Experimental and numerical studies of insulating layers effect on liquid pipelines leakage in chemical plants. Process Saf. Environ. Prot. 147, 888–899. https://doi.org/10.1016/j.psep.2021.01.014.
G189, A.S., 2007. Standard Guide for Laboratory Simulation of Corrosion Under Insulation. American Society for Testing and Materials (ASTM). ⟨https://www.astm.org/g0189-07r21e01.html⟩.
Geary, W., 2013. Analysis of a corrosion under insulation failure in a carbon steel refinery hydrocarbon line. Case Studies in. Eng. Fail. Anal. 1, 249–256. https://doi.org/10.1016/j.csefa.2013.09.001. ⟨https://linkinghub.elsevier.com/retrieve/pii/S2213290213000448⟩.
Hagentoft, C.E., Kalagasidis, A.S., Adl-Zarrabi, B., Roels, S., Carmeliet, J., Hens, H., Grunewald, J., Funk, M., Becker, R., Shamir, D., Adan, O., Brocken, H., Kumaran, K., Djebbar, R., 2004. Assessment Method of Numerical Prediction Models for Combined Heat, Air and Moisture Transfer in Building Components: Benchmarks for One-dimensional Cases. J. Therm. Envel. Build. Sci. 27, 327–352. https://doi.org/10.1177/1097196304042436.
Hall, C., 1977. Water movement in porous building materials—I. Unsaturated flow theory and its applications. Build. Environ. 12, 117–125. https://doi.org/10.1016/0360-1323(77)90040-3. ⟨https://www.sciencedirect.com/science/article/pii/0360132377900403⟩.
Hall, C., 1989. Water sorptivity of mortars and concretes: a review. Mag. Concr. Res. 41, 51–61. https://doi.org/10.1680/macr.1989.41.147.51.
Hall, C., Tse, T.K.M., 1986. Water movement in porous building materials—VII. The sorptivity of mortars. Build. Environ. 21, 113–118. https://doi.org/10.1016/0360-1323(86)90017-X. ⟨https://www.sciencedirect.com/science/article/pii/036013238690017X⟩.
Haraldsen, K., 2010. Corrosion Under Insulation - Testing Of Protective Systems At High Temperatures. In: NACE CORROSION 2010. OnePetro (https://dx.doi.org/).
Hart, T. 2014. Neutron backscatter versus gamma transmission analysis for coke drum applications. ⟨https://tools.thermofisher.com/content/sfs/brochures/EPM-ANCoker-0215.pdf⟩ (accessed on 20 December 2021).
Hillier, A., Khan, F., Caines, S., 2021. Pitting and Corrosion Rates of Coated, Uncoated, and Insulated A333 Steel Pipelines in Marine Harsh Environment. Am. Soc. Mech. Eng. Digit. Collect. https://doi.org/10.1115/OMAE2021-62461. In: ⟨https://asmedigitalcollection.asme.org/OMAE/proceedings/OMAE2021/85123/V002T02A033/1121303⟩.
Hoffman, A., 2019. Moisture as a cause of corrosion under insulation. Waste + Water Manag. Aust. 46, 44–48. https://doi.org/10.3316/INFORMIT.589347952742194.
Ioannou, I., Hamilton, A., Hall, C., 2008. Capillary absorption of water and n-decane by autoclaved aerated concrete. Cem. Concr. Res. 38, 766–771. https://doi.org/10.1016/j.cemconres.2008.01.013. ⟨https://www.sciencedirect.com/science/article/pii/S0008884608000409⟩.
Jerman, M., Černý, R., 2012. Effect of moisture content on heat and moisture transport and storage properties of thermal insulation materials. Energy Build. 53, 39–46. https://doi.org/10.1016/j.enbuild.2012.07.002. ⟨https://www.sciencedirect.com/science/article/pii/S0378778812003143⟩.
Jiričková, M., Černý, R., 2006. Effect of hydrophilic admixtures on moisture and heat transport and storage parameters of mineral wool. Constr. Build. Mater. 20, 425–434. https://doi.org/10.1016/j.conbuildmat.2005.01.055. ⟨https://www.sciencedirect.com/science/article/pii/S0950061805000723⟩.
Jones, R., Simonetti, F., Lowe, M., Bradley, I., 2012. Use of microwaves for the detection of water as a cause of corrosion under insulation. J. Nondestruct. Eval. 31, 65–76. https://doi.org/10.1007/s10921-011-0121-9.
Kane, R.D., Chauviere, M., Chustz, K., 2008. Evaluation Of Steel And TSA Coating In A Corrosion Under Insulation (CUI) Environment. In: NACE CORROSION 2008. OnePetro. In: ⟨https://onepetro.org/NACECORR/proceedings-abstract/CORR08/All-CORR08/118701⟩.
Kontogeorgis, G.M., Kiil, S., 2016. Introduction to Applied Colloid and Surface Chemistry, 1st ed. John Wiley & Sons, United Kingdom.
Kumar, M.S., Sujata, M., Venkataswamy, M.A., Bhaumik, S.K., 2008. Failure analysis of a stainless steel pipeline. Eng. Fail. Anal. 15, 497–504. https://doi.org/10.1016/j.engfailanal.2007.05.002. ⟨https://www.sciencedirect.com/science/article/pii/S1350630707000921⟩.
de Landtsheer, G., 2020. Corrosion Under Insulation (CUI) Guidelines - Technical Guide for Managing CUI, 3rd ed. Elsevier. European Federation of Corrosion Publications Number 55 ⟨https://www.elsevier.com/books/corrosion-under-insulation-cui-guidelines/de-landtsheer/978-0-12-823332-0⟩. (Ed.).
Langøy, M.A., Hörnlund, E., Næss, O.J., Hinderaker, R.H., 2017. Corrosion Processes Relevant to the Integrity of Oil and Gas Facilities. Open Conf. Proc. J. 8 https://doi.org/10.2174/2210289201708010014. In: ⟨https://benthamopen.com/ABSTRACT/TOPROCJ-8-14⟩.
Mansfeld, F., 1979. Atmospheric corrosion rates, time-of-wetness and relative humidity. Mater. Corros. 30, 38–42. https://doi.org/10.1002/maco.19790300105.
Miyashita, J., 2017. Performance of Three Types of Coatings in a Simulated Corrosion under Insulation Condition. OnePetro. In: ⟨https://onepetro.org/NACECORR/proceedings/CORR17/All-CORR17/NACE-2017-9296/125533⟩.
Miyashita, J., Tsuda, T., Horikiri, K., 2016. Evaluation of Protective Coating Performance in a Cyclic-Temperature Environment. OnePetro. In: ⟨https://onepetro.org/NACECORR/proceedings-abstract/CORR16/All-CORR16/123548⟩.
Mohamad, A.A., Bennacer, R., 2001. Natural convection in a confined saturated porous medium with horizontal temperature and vertical solutal gradients. Int. J. Therm. Sci. 40, 82–93. https://doi.org/10.1016/S1290-0729(00)01182-0. ⟨https://www.sciencedirect.com/science/article/pii/S1290072900011820⟩.
Nellis, G.F., Klein, S.A., 2020. Introduction to Engineering Heat Transfer. Cambridge University Press.
Petty, G.W., 2008. A First Course in Atmospheric Thermodynamics, 1st ed. Sundog Publishing.
Philip, J.R., Vries, D.A.D., 1957. Moisture movement in porous materials under temperature gradients. Eos, Trans. Am. Geophys. Union 38, 222–232. https://doi.org/10.1029/TR038i002p00222.
Pojtanabuntoeng, T., Machuca, L.L., Salasi, M., Kinsella, B., Cooper, M., 2015. Influence of Drain Holes in Jacketing on Corrosion Under Thermal Insulation. Corrosion 71, 1511–1520. https://doi.org/10.5006/1861. ⟨https://www.proquest.com/docview/2421630777/abstract/E3CA24B4FFB348B6PQ/1⟩.
Ramirez-Ledesma, A., Juarez-Islas, J., 2022. Modification of the remaining useful life equation for pipes and plate processing of offshore oil platforms. Process Saf. Environ. Prot. 157, 429–442. https://doi.org/10.1016/j.psep.2021.11.022.
Rana, A.R.K., Yang, M., Umer, J., Veret, T., Brigham, G., 2021. Influence of Robust Drain Openings and Insulation Standoffs on Corrosion Under Insulation Behavior of Carbon Steel. Corrosion 77, 681–692. https://doi.org/10.5006/3749.
Roberge, P.R., 2008. Corrosion engineering: principles and practice. McGraw-Hill, New York.
Roels, S., Carmeliet, J., Hens, H., Adan, O., Brocken, H., Cerny, R., Pavlik, Z., Hall, C., Kumaran, K., Pel, L., Plagge, R., 2004. Interlaboratory Comparison of Hygric Properties of Porous Building Materials. J. Therm. Envel. Build. Sci. 27, 307–325. https://doi.org/10.1177/1097196304042119.
Roffey, P., Davies, E.H., 2014. The generation of corrosion under insulation and stress corrosion cracking due to sulphide stress cracking in an austenitic stainless steel hydrocarbon gas pipeline. Eng. Fail. Anal. 44, 148–157. https://doi.org/10.1016/j.engfailanal.2014.05.004. ⟨https://www.sciencedirect.com/science/article/pii/S1350630714001514⟩.
Schoon, A., Fjellanger, R., Kjeldsen, M., Goss, K.U., 2014. Using dogs to detect hidden corrosion. Appl. Anim. Behav. Sci. 153, 43–52. https://doi.org/10.1016/j.applanim.2014.01.001. ⟨https://www.sciencedirect.com/science/article/pii/S0168159114000021⟩.
Shrestha, S., Antretter, F., Desjarlais, A.O., Venkateswaran, S.P. 2021.Using Models to Predict the Hygrothermal Performance of Equipment and Piping Insulation. Technical Report. Oak Ridge National Lab. (ORNL), Oak Ridge, TN (United States). ⟨https://www.osti.gov/biblio/1827054⟩.
Simonetti, F., Nagy, P.B., Bejjavarapu, S.M., Instanes, G., Pedersen, A.O. 2015.Long-Range Microwave Detection of Wet Insulation for CUI Mitigation, OnePetro. ⟨https://onepetro.org/NACECORR/proceedings-abstract/CORR15/All-CORR15/123376⟩.
Sophian, A., Tian, G., Fan, M., 2017. Pulsed Eddy Current Non-destructive Testing and Evaluation: A Review. Chin. J. Mech. Eng. 30, 500–514. https://doi.org/10.1007/s10033-017-0122-4.
Tariku, F., Kumaran, K., Fazio, P., 2010b. Transient model for coupled heat, air and moisture transfer through multilayered porous media. Int. J. Heat. Mass Transf. 53, 3035–3044.
Tariku, F., Kumaran, K., Fazio, P., 2010a. Integrated analysis of whole building heat, air and moisture transfer. Int. J. Heat. Mass Transf. 53, 3111–3120. https://doi.org/10.1016/j.ijheatmasstransfer.2010.03.016. ⟨https://www.sciencedirect.com/science/article/pii/S0017931010001493⟩.
Trevisan, O.V., Bejan, A., 1985. Natural convection with combined heat and mass transfer buoyancy effects in a porous medium. Int. J. Heat. Mass Transf. 28, 1597–1611. https://doi.org/10.1016/0017-9310(85)90261-3. ⟨https://www.sciencedirect.com/science/article/pii/0017931085902613⟩.
Vejmelková, E., Pavlíková, M., Jerman, M., Černý, R., 2009. Free Water Intake as Means of Material Characterization. J. Build. Phys. 33, 29–44. https://doi.org/10.1177/1744259109104069.
Xu, P., Sasmito, A.P., Mujumdar, A.S., 2020. Heat and Mass Transfer in Drying of Porous Media, 1st ed. CRC Press, Boca Raton.
Yadav, A.P., Nishikata, A., Tsuru, T., 2004. Electrochemical impedance study on galvanized steel corrosion under cyclic wet-dry conditions–influence of time of wetness. Corros. Sci. 46, 169–181. https://doi.org/10.1016/S0010-938X(03)00130-6. ⟨https://www.sciencedirect.com/science/article/pii/S0010938X03001306⟩.
Yang, Z., Weiss, W., Olek, J., 2006. Water Transport in Concrete Damaged by Tensile Loading and Freeze-Thaw Cycling. J. Mater. Civ. Eng. 18 https://doi.org/10.1061/(ASCE)0899-1561(2006)18:3(424).
Zhu, W., Rose, J.L., Barshinger, J.N., Agarwala, V.S., 1998. Ultrasonic Guided Wave NDT for Hidden Corrosion Detection. Res. Nondestruct. Eval. 10, 205–225. https://doi.org/10.1080/09349849809409629.